Effects of Polarizability and Charge Transfer on Water Dynamics and the Underlying Activation Energies

Steven W. Rick[1, a)] and Ward H. Thompson[2, b)]
[1)] *Department of Chemistry, University of New Orleans, New Orleans, LA 70148, USA*
[2)] *Department of Chemistry, University of Kansas, Lawrence, KS 66045, USA*

(Dated: 20 May 2023)

A large number of force fields have been proposed for describing the behavior of liquid water within classical atomistic simulations, particularly molecular dynamics. In the past two decades, models that incorporate molecular polarizability and even charge transfer have become more prevalent, in attempts to develop more accurate descriptions. These are frequently parameterized to reproduce the measured thermodynamics, phase behavior, and structure of water. On the other hand, the dynamics of water is rarely considered in construction of these models, despite its importance in their ultimate applications. In this Paper, we explore the structure and dynamics of polarizable and charge-transfer water models, with a focus on timescales that directly or indirectly relate to hydrogen bond (H-bond) making and breaking. Moreover, we use the recently developed fluctuation theory for dynamics to determine the temperature dependence of these properties to shed light on the driving forces. This approach provides key insight into the timescale activation energies through a rigorous decomposition into contributions from the different interactions, including polarization and charge transfer. The results show that charge transfer effects have a negligible effect on the activation energies. Further, the same tension between electrostatic and van der Waals interactions that is found in fixed-charge water models also governs the behavior of polarizable models. The models are found to involve significant energy-entropy compensation, pointing to the importance of developing water models that accurately describe the temperature dependence of water structure and dynamics.

I. INTRODUCTION

The barriers for translational and rotational motion of a molecule in liquid water are established by the potential energy surface. Many simple yet accurate models of water treat these interactions as a sum of two parts, the electrostatic interactions between sites with partial charges and a Lennard-Jones interaction, usually between oxygen atoms,[1–6] representing short-ranged repulsions and longer-ranged dispersion. Many dynamical properties of water are associated with hydrogen-bond (H-bond) making and breaking and the activation energies in these models are largely determined by a competition between the electrostatic and repulsive Lennard-Jones interactions.[7–10] The former, which represent the driving force for H-bonding, are dominant, but diminished by the latter, which favor weaker H-bonding structures.

Other water models treat electronic polarizability[11–17] and charge transfer.[18–24] Several studies have shown charge transfer is implicated in translation motion of liquid water.[25–28] The inclusion of charge transfer is necessary to match the infrared[25–28] and Raman[27,28] peak at 200 cm^{-1} that is associated with hindered translational motion. In general, polarizable and non-polarizable potentials give similar results for diffusion and rotational constants, often because dynamical properties are used to fit the models. A few studies suggest some differences between polarizable and non-polarizable models. Xu *et al.*, found that polarizability strengthens hydrogen bonds and slows down H-bond kinetics by increasing the free energy barrier for breaking hydrogen bonds.[29] A similar result, with higher barriers for hydrogen bond jumps with polarizable models, was found for water in confined environments.[30] Polarizable potentials not only tend to have stronger electrostatic interactions, with average dipoles that are larger than non-polarizable models, but also have electrostatic interactions which change in response to the environment. These two aspects of polarizable models have opposing effects on dynamics. By allowing the dipole to respond to the different environments at dynamical barriers, these barriers may have lower energies.[31] The faster dynamics through the polarization response is suggested by the results of the non-polarizable Watanabe-Klein model, which has charges that give a dipole moment similar to polarizable models.[32] This model gives translational and rotational timescales that are too slow by about a factor of two.[32]

The effects of polarizability and charge transfer interactions on the dynamics of water is the focus of the present work. Using two different polarizable models, with different approaches to treating polarizability,[12,15] and versions of those models which include charge transfer,[23,24] this paper uses the fluctuation theory for dynamics[7,8,33] to determine the activation energies for translational diffusion, rotational dynamics, and

[a)] Electronic mail: srick@uno.edu
[b)] Electronic mail: wthompson@ku.edu

hydrogen-bond exchange dynamics. This approach allows contributions from the different parts of the potentials, including polarizability and charge transfer, to be determined. The energetic contributions to the structure of water are also calculated.

II. THEORY

In this work, we use the recently developed fluctuation theory for dynamics[7,8,33] that permits the calculation of activation energies from simulations at a single temperature. This is accomplished by determining the analytical derivative of a timescale (or, indeed, the underlying time correlation function itself) rather than the numerical derivative obtained in a traditional Arrhenius analysis.

The essence of the method can be seen by considering a general statistical mechanical average of a property, f, that can, in general, depend on a time interval:

$$\langle f(t)\rangle = \frac{1}{Qh^F}\int d\mathbf{q}\int d\mathbf{p}\, e^{-\beta H(\mathbf{p},\mathbf{q})}\, f(\mathbf{p},\mathbf{q};t), \qquad (1)$$

where $\mathbf{q}$ and $\mathbf{p}$ are the system coordinates and momenta, H the Hamiltonian, $\beta = 1/k_bT$ with k_b Boltzmann's constant, Q the canonical partition function, and F the number of degrees-of-freedom. The temperature only appears in this average in the Boltzmann factor, $e^{-\beta H}$, and the normalizing partition function, Q. Thus, taking the derivative of the average with respect to T or, more conveniently, β, yields only two terms:

$$\begin{aligned}\frac{\partial\langle f(t)\rangle}{\partial\beta} &= \langle H\rangle\,\langle f(t)\rangle - \langle H(0)\, f(t)\rangle,\\ &= -\langle \delta H(0)\, f(t)\rangle,\\ &\equiv -f_H(t). \end{aligned} \qquad (2)$$

Here, we have used the fact that $(\partial \ln Q/\partial\beta) = \langle H\rangle$ and defined the fluctuation in the total system energy at $t = 0$ as $\delta H(0) = H(0) - \langle H\rangle$.

A focus of this study is to determine how non-additivity in the molecular interactions influence dynamical properties. We use two different polarizable models, the TIP4P-FQ model,[12] which treats polarizability using dynamical charges that respond to the electric fields of other molecules, and the SWM4+NDP Drude[15] model, which uses a charge site connected by a harmonic spring to the oxygen atom to treat dipole polarizablity. Charge transfer effects have been added to both models, using the Discrete Charge Transfer (DCT) approach. In these models (TIP4P-FQ+DCT[23] and Drude-DCT[24]), a discrete amount of charge in transferred for each hydrogen bond formed. This amount of charge, $0.02e$, consistent with the results of electronic structure calculations, is transferred to the H-bond donor from the acceptor. The hydrogen bond donor becomes more electronegative and so attracts electron density. The energy associated with this charge transfer, V_{CT}, is -0.15 kcal/mol for each hydrogen bond, fitted to the results of *ab initio* calculations.[34] This energy is partially offset by a decrease in the Coulombic energy from the reduced charges of the H-bonded pair. The amount of charge transfer and therefore V_{CT} is dependent on the hydrogen-oxygen distance and goes to zero at 2.8 Å, as indicated by electronic structure results.[35]

In this context, a critical advantage of the fluctuation theory for dynamics approach is the ability to obtain key mechanistic information. In particular, the fluctuation in the total energy can be decomposed into contributions from different motions and interactions of the system. This partitioning does not rely on the potential being pairwise additive. For the polarizable and charge transfer water models considered here, for example, we can write

$$\begin{aligned}\delta H(0) = \delta KE(0) + \delta V_{LJ}(0)\\ + \delta V_{Coul}(0) + \delta V_{Pol}(0) + \delta V_{CT}(0),\end{aligned} \qquad (3)$$

where KE represents the total system kinetic energy and V_{LJ}, V_{Coul}, V_{Pol}, and V_{CT} are the Lennard-Jones, Coulombic, polarization, and charge transfer potential energies. Note that V_{Coul} represents the electrostatic energy of the charges obtained after polarization and V_{Pol} the energetic cost associated with that polarization. Substituting Eq. (3) for $\delta H(0)$ in the derivative given in Eq. (2) gives contributions to that derivative associated with each of the interactions and the kinetic energy. That is, we can write

$$\begin{aligned}f_H(t) = f_{KE}(t) + f_{LJ}(t)\\ + f_{Coul}(t) + f_{Pol}(t) + f_{CT}(t),\end{aligned} \qquad (4)$$

where, for example, $f_{LJ}(t) = \langle \delta V_{LJ}(0)\, f(t)\rangle$. As we have previously shown,[7,8] these contributions can be extended to determine an analogous rigorous decomposition of the activation energy.

We apply this fluctuation theory for dynamics approach to key properties for water dynamics including diffusion, $f(t) = MSD(t) = |\vec{r}(t) - \vec{r}(0)|^2$, OH reorientation, $f(t) = C_2(t) = P_2[\vec{e}_{OH}(t)\cdot\vec{e}_{OH}(0)]$ where P_2 is the second Legendre polynomial, and the exchange of H-bond acceptors, $f(t) = C_{ab}(t) = n_a(0)\, n_b(t)$ where $n_x = 1$ if an OH is H-bonded to acceptor x and $n_x = 0$ otherwise. In addition, the driving forces for water structure were considered by taking $f(t)$ to be the static radial distribution function.

III. COMPUTATIONAL METHODS

All simulations were conducted with in-house code. The simulations used 343 water molecules, equilibrated at a temperature of 300 K, using a Nosé-Hoover thermostat, and a pressure of 1 bar, using an Anderson barostat.[36] Ewald summations were used for the electrostatic interactions. Rigid bonds are constrained with SHAKE[36] and a time step of 1 fs was used. For the TIP4P-FQ and TIP4P-FQ+DCT models,

charges were treated as dynamical variables and propagated with the extended Langrangian formalism, as described previously.[12,23] For the SWM4+NDP Drude[15] and Drude-DCT[24] models, the Drude particle is given a mass of 0.4 amu, which is subtracted from the mass of the oxygen atom, and Drude positions are propagated as described by Lamoureux and Roux.[37]

The fluctuation theory calculations were implemented as follows. For each water model five sequential NVT trajectories were propagated with restart files written every 1 ps. The latter were used to launch 500 NVE trajectories (giving 2500 in total for each model), from which the dynamics and derivatives, *via* Eq. (2), were computed. This approach yields an ensemble of trajectories that have dynamics unaffected by thermostatting but with energies consistent with a canonical distribution. (It has the added advantage that the NVE trajectories are embarrassingly parallel.) Errors in the computed results were obtained by block averaging using 5 blocks (each block representing 500 NVE trajectories) and are reported as 95% confidence intervals using the Student's t-distribution.[38]

IV. RESULTS AND DISCUSSION

A. Water Structure

We first consider the structural features of liquid water predicted by the different models based on the oxygen-oxygen (O-O) radial distribution function (RDF),

$$g(r) = \frac{V}{N^2}\left\langle \sum_i \sum_{j\neq i} \delta(r - |\vec{r}_{ij}|) \right\rangle, \tag{5}$$

where V is the system volume, N the number of of molecules, and $\vec{r}_{ij}$ the vector from the oxygen atom of molecule i to the oxygen atom of molecule j. While, unlike the general case described in Sec. II, this property is independent of time, the result for the β derivative is the same:[39]

$$\frac{\partial g(r)}{\partial \beta} = -\frac{V}{N^2}\left\langle \delta H \sum_i \sum_{j\neq i} \delta(r - |\vec{r}_{ij}|) \right\rangle \equiv -g_H(r). \tag{6}$$

Additionally, the same decompositions shown in Eq. (3) are used obtain the contributions of the different interactions to the temperature derivative. This gives insight into the driving forces that determine the water structure and does not assume pairwise additivity. (Note that because $g(r)$ is independent of momenta, there is no contribution from the kinetic energy.)

The O-O RDFs for the four water models are shown in Fig. 1 along with their derivatives (plotted as $-g_H(r)$). In addition, the contributions from the different interaction terms, $-g_X(r)$, in the force fields are shown. The four water models yield fairly similar water structure. The first peak in the RDF, giving the location of the first solvation shell, is ~ 2.8 Å in all cases and the peak height of ~ 2.9 is also nearly the same. The two TIP4P-FQ-based models give a slightly less structured (smaller amplitude peaks), but more compact, second solvation shell compared to the SWM4+NDP and, to a greater extent, the Drude-CT model.

Despite the similarity of the RDFs, the models exhibit temperature dependences that are dramatically different quantitatively. Qualitatively, the derivative $-g_H(r)$ oscillates around zero with an amplitude that decreases with increasing distance. In particular, $\partial g(r)/\partial\beta$ is positive over the first rise of the RDF corresponding to the first solvation shell, passes through zero near the $g(r)$ peak and is negative over the remainder of the first solvation shell. This indicates that as temperature increases (decreases), the first peak will shift to larger (shorter) distances. However, the derivative is of significantly larger magnitude for the TIP4P-FQ and TIP4P-FQ-DCT models compared to the SWM4+NDP and Drude-DCT models. In particular, $-g_H(r)$ has a maximum at 2.7 Å of 10 kcal/mol for the former two force fields compared to ~ 4 kcal/mol for the latter ones. Similarly the minimum values around 3.1 Å are smaller by more than a factor of two for the SWM4+NDP and Drude-DCT force fields compared to the TIP4P-FQ-based ones. Implications for this are evident in the related internal energy profiles discussed below.

It is useful to directly examine the thermodynamic driving forces for the RDF. In particular, an effective free energy as a function of the O-O distance is given by the potential of mean force,

$$\begin{aligned} PMF(r) &= -k_b T \ln g(r) \\ &= \Delta U(r) - T\Delta S_{PMF}(r) \end{aligned} \tag{7}$$

Note that this is not the full free energy, $\Delta A(r) = PMF(r) - 2k_bT\ln r$, which differs by an entropic term accounting for the greater available volume for two molecules as the distance between them increases. As noted in Eq. (7), the PMF is composed of both internal energy and entropy contributions; the full entropy is $\Delta S(r) = \Delta S_{PMF}(r) - 2k_bT\ln r$. We have previously shown[39] that the internal energy can be obtained straightforwardly from the temperature derivative as

$$\Delta U(r) = \frac{g_H(r)}{g(r)}, \tag{8}$$

and then $\Delta S_{PMF}(r)$ can be calculated from Eq. (7).

The PMF, internal energy, and entropy profiles are shown for the four water models in Fig. 2. Because the PMFs are a direct mapping of the RDFs, they exhibit the same comparative behavior discussed for the latter above. Most notably, the Drude-DCT shows a somewhat larger barrier for a water molecule to move between the first and second solvation shells compared to the TIP4P-FQ-based models, which give nearly identical results.

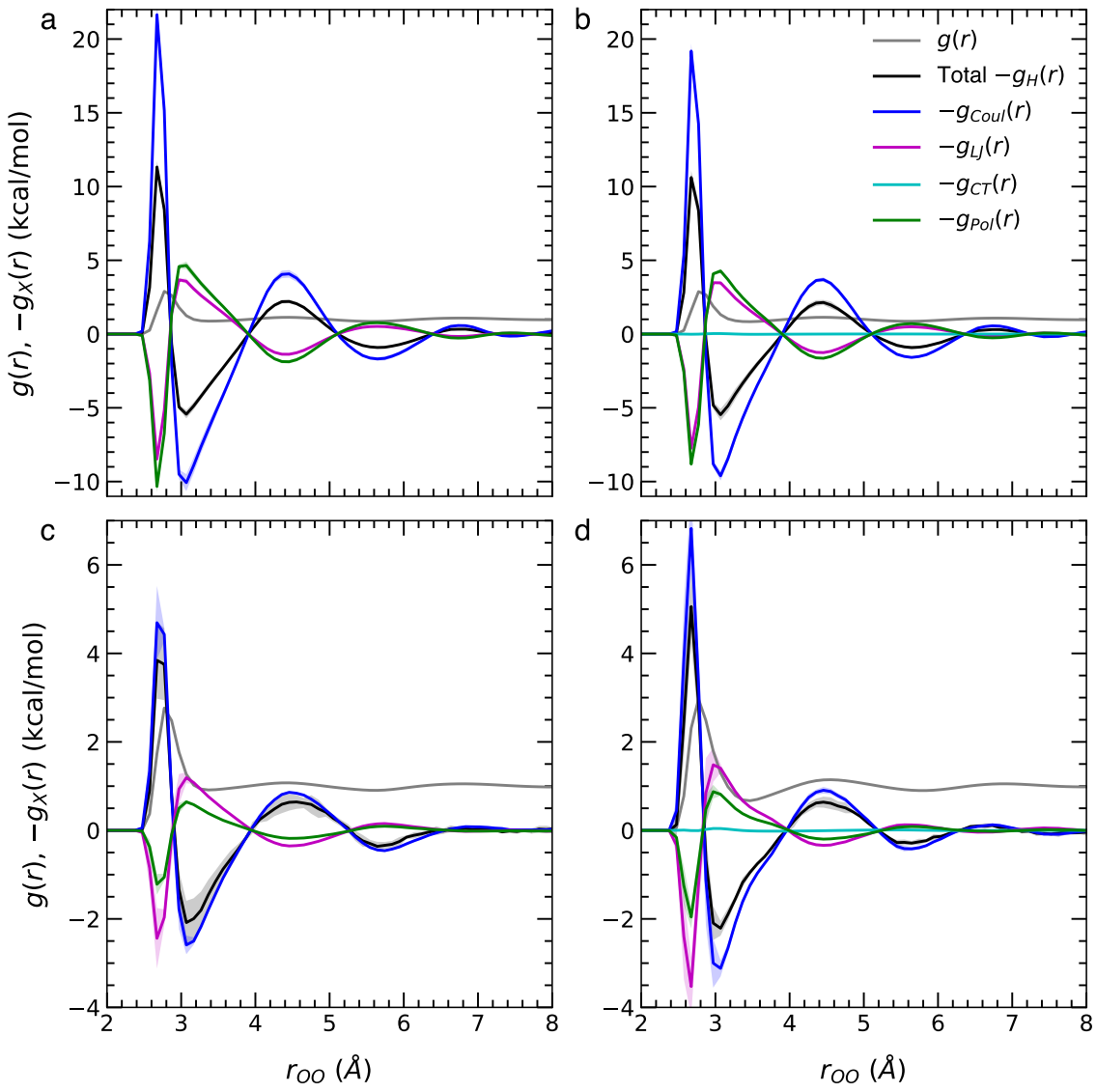

FIG. 1: The O-O radial distribution function, $g(r)$, is plotted as a function of distance along with the derivative, shown as $-g_H(r) = \partial g(r)/\partial\beta$, and its contributions from the different interactions present. Results are shown for the a) TIP4P-FQ, b) TIP4P-FQ-DCT, c) SWM4+NDP, and d) Drude-DCT models. Shaded areas represent the 95% confidence intervals.

The energetic and entropic contributions, Fig. 2b,c, are quite a different story. The TIP4P-FQ-based models have internal energy profiles that are strongly modulated, *e.g.*, the barrier to move from the first to the second solvation shell around a water molecule is $\Delta U^{\ddagger}_{1\to 2} \simeq$ 7 kcal/mol. This is ten times larger than the barrier in the PMF for those models and more than three times larger than the internal energy barrier for the Drude-DCT force field. The former is a result of significant energy-entropy compensation. The entropy profiles for the TIP4P-FQ-based models are also more strongly modulated compared to the Drude-DCT model, but in all cases the entropic contributions largely cancel the internal energy leading to much more modest changes in the PMF (or free energy). However, it is important to note that it is the internal energy that determines how the RDF changes with temperature through a van't Hoff relationship,[39] so that the TIP4P-FQ-based models should predict much larger structural changes with temperature compared to the Drude-DCT description.

B. Hydrogen-Bond Exchange Dynamics

The central process in water dynamics is the making and breaking of H-bonds. The exchange of H-bond partners has been explicitly shown to underlie water reorientation[40,41] and diffusion[42] (though interestingly,

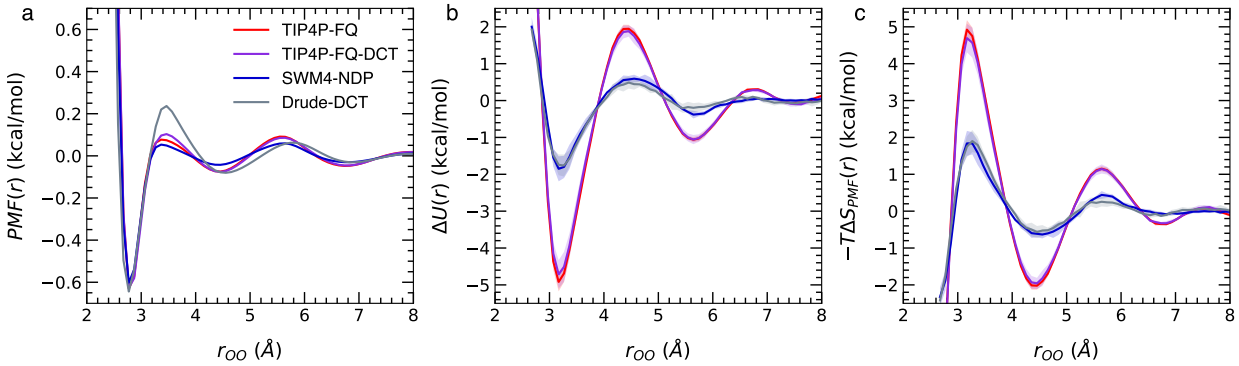

FIG. 2: The a) potential of mean force (PMF), b) internal energy profile, $\Delta U(r)$, and c) PMF entropy profile, $-T\Delta S_{PMF}(r)$, associated with the O-O radial distribution function are plotted as a function of distance for the four water models. Shaded areas represent the 95% confidence intervals.

not spectral diffusion[43]). This exchange can be viewed as analogous to a chemical reaction in which an OH group switches, or "jumps," from one H-bond acceptor to another. This event can be characterized by a rate constant, k_0, or, more typically, by a jump time $\tau_0 = 1/k_0$. Given the key role of H-bond exchanges, the jump time is perhaps the most fundamental dynamical quantity of liquid water.

It can be calculated from a time correlation function (TCF) based on a stable-states picture,[44]

$$C_{ab}(t) = \langle n_a(0)\, n_b(t)\rangle, \tag{9}$$

where a and b label two different H-bond acceptors. Here, $n_x(t) = 1$ for an OH that is donating an H-bond to accepting water molecule x at time t and $n_x(t) = 0$ otherwise. For each OH we can label its H-bond acceptor at a time $t = 0$ as molecule a and $C_{ab}(t) = 0$ because $n_x(0) = 0$ for all other H-bond acceptors. As time elapses and the OH group switches to a new acceptor, which we label b, $C_{ab}(t) = 1$ because $n_a(0) = 1$ but also $n_b(t) = 1$. We use absorbing boundary conditions, *i.e.*, $n_b(t) = 1$ for all times after the H-bond has switched; this ensures the dynamics captured by $C_{ab}(t)$ report only on a single H-bond exchange process, independent of transient H-bond breaks or returns to the original H-bond acceptor. It can be shown that this TCF exhibits an exponential rise with a time constant that is the jump time:[40,41]

$$e^{-t/\tau_0} = 1 - C_{ab}(t). \tag{10}$$

In practice we fit $1 - C_{ab}(t)$ to a single exponential $A_0 e^{-t/\tau_0}$ to account for a small amplitude part of the decay at early times unrelated to the jump time.

In the present work, we use stringent geometric criteria to define an H-bond: $r_{OO} \leq 3.1$ Å, $r_{H\cdots O} \leq 2.0$ Å, and $\theta_{H-O\cdots O} \leq 20°$. The H-bond jump TCFs, Eq. (9), for the four water models considered here are plotted in Fig. 3a and the jump times obtained from them using Eq. (10) are given in Table I. The TIP4P-FQ, TIP4P-FQ-DCT, and Drude-DCT models give relatively similar dynamics, with jump times all between $\sim 3.8 - 4.2$ ps. There is currently no experimental approach for measuring τ_0 in neat water. However, these times are slower than that found for the SWM4-NDP force field and a range of rigid and flexible fixed-charge models investigated previously[9] for which jump times are between 2.25 and 3.66 ps. The longest of these corresponds to the TIP4P/2005 model that is the fixed charge model that gives the best overall agreement with experimental timescales, activation energies, and activation volumes.[9] Three-body models developed by Tainter *et al.*[45,46], which also yield generally good agreement with experiments, give even longer jump times of ~ 4.4 ps.

One difference between the TIP4P-FQ, TIP4P-FQ-DCT, and Drude-DCT models and the SWM4-NDP model, relevant to these timescales, is that SWM4-NDP has gas-phase charges on the hydrogens and the M-site; the polarization is only through the Drude particle. The FQ models have charges that are polarized, so hydrogen and M-site charges are enhanced. The partitioning of the charge transferred in the Drude-DCT, based on quantum calculations of the dimer, changes the charges from the gas-phase values, resulting in more (about $-0.06e$) negative charge on the M-site, and correspondingly ($0.03e$) more positive charge on the hydrogens, and the dipole is larger by 0.1 Debye for the Drude-DCT compared to the SWM4-NDP model. This makes the hydrogens on the SWM4-NDP model less strongly interacting, speeding up reorientation.

The activation energy associated with the jump time can be obtained from the fluctuation theory approach. Namely, we calculate the weighted TCF,

$$C_{ab,H}(t) = \frac{\partial[1 - C_{ab}(t)]}{\partial\beta} = \langle \delta H(0)\, n_a(0)\, n_b(t)\rangle. \tag{11}$$

This TCF is fit to the derivative of $A_0 e^{-t/\tau_0}$ with respect to β, with A_0 and τ_0 fixed to the values determined by fitting $1 - C_{ab}(t)$.[33] This yields $\partial A_0/\partial\beta$ and $\partial\tau_0/\partial\beta$ and the latter is used to calculate the jump time activation energy. The TCFs for all four water models are plotted in Fig. 3b along with their fits. (Note that the activation

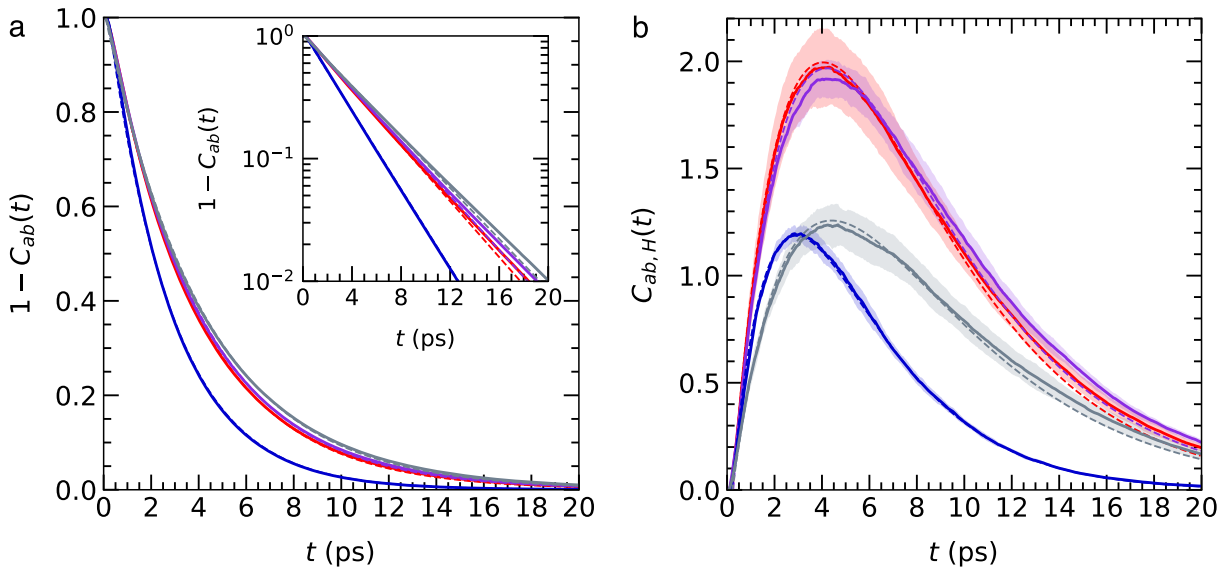

FIG. 3: The a) H-bond exchange TCF, $1 - C_{ab}(t)$, and b) derivative of this TCF, $C_{ab,H}$ given in Eq. (11) are plotted as a function of time for the TIP4P-FQ (red), TIP4P-FQ-DCT (violet), SWM4-NDP (blue), and Drude-DCT (grey) models. Dashed lines of the same color show fits as described in the text. Inset in a) shows the TCFs on a semi-log scale. Shaded areas represent the 95% confidence intervals.

Timescale	TIP4P-FQ	TIP4P-FQ-DCT	SWM4-NDP	Drude-DCT	TIP4P/2005[9]	Expt.[47–50]
τ_0	3.82_2	3.95_1	2.71_1	4.18_2	3.657_7	–
τ_2	3.43_3	3.63_4	2.29_7	4.40_2	3.165_8	2.6
D	1.86_1	1.77_1	2.81_2	1.64_1	2.030_4	2.30

TABLE I: H-bond jump time τ_0, OH reorientation time τ_2, and diffusion coefficients, D, for different polarizable and charge-transfer water models; times are in ps, and diffusion coefficients are in 10^{-5} cm^2/s. Subscripts indicate uncertainties in the trailing digit(s). Note that the D values have not been corrected for finite-size effects.[51–53]

energy can also be found directly from these plots[33] as $C_{ab,H}(t)$ reaches a maximum at the jump time and the peak height is equal to $e^{-1}E_a$.)

The jump time activation energies, $E_{a,0}$, are given in Table II along with the contributions from the kinetic energy and the different interactions present in the force fields. These data are also plotted in Fig. 4. Results for the TIP4P/2005 model are shown for comparison along with experimental values where available. The $E_{a,0}$ values mirror the results for the RDF derivatives. Namely, the TIP4P-FQ and TIP4P-FQ-DCT models give significantly higher activation energies, $E_{a,0} \simeq 5.5$ kcal/mol, compared to the SWM4-NDP and Drude-DCT models. The latter two, however, give values that are in general accord with the ranges found in previous work for fixed-charge and three-body force fields for which $E_{a,0} = 2.7 - 4.1$ kcal/mol.[60] These results indicate that the TIP4P-FQ-based models predict much stronger temperature dependence of H-bond exchanges. However, the *free* energy barrier for H-bond exchanges is related to the O-O RDF[61] and, as noted above, these are quite similar for the different models. This indicates that the activation entropy for H-bond exchanges balances the activation energies (see Fig. 2) at room temperature, which would then no longer be the case at other temperatures, both higher and lower.

The contributions of the different interaction types to $E_{a,0}$ are also revealing. First we note that the kinetic energy contribution is nearly the same for all models, ~ 1 kcal/mol. The charge transfer component, included only for the TIP4P-FQ-DCT and Drude-DCT models, is essentially negligible, < 0.03 kcal/mol. This is somewhat surprising as it suggests that the energy associated with charge transfer is not strongly different between the transition state for H-bond exchanges. Breaking an H-bond increases the charge transfer energy by $+0.15$ kcal/mol in the CT models. Note that this transition state is effectively a bifurcated H-bond in which the donating H atom is equidistant between the oxygen atoms of the original and new H-bond acceptors.[40,41] This geometry of the transition state has the H atom at a distance of about 2.4 Å from both oxygen atoms. The CT models turn off the charge transfer over a distance from 2.3 to 2.8 Å, so at the transition state there will be charge transfer be-

Activation Energy	Component	TIP4P-FQ	TIP4P-FQ-DCT	SWM4-NDP	Drude-DCT	TIP4P/2005[9]	Expt.
$E_{a,0}$	Total	5.53_{22}	5.51_{14}	3.23_{6}	3.53_{14}	3.63_{5}	–
	Kinetic Energy	1.01_{11}	1.02_{11}	1.07_{3}	0.95_{6}	1.04_{4}	
	Lennard-Jones	-4.87_{60}	-4.83_{32}	-1.00_{8}	-1.29_{9}	-1.10_{6}	
	Coulombic	$17.1_{1.5}$	16.5_{8}	4.07_{18}	5.17_{20}	3.69_{8}	
	Polarization	-7.68_{69}	-7.20_{36}	-0.91_{5}	-1.27_{4}	–	
	Charge Transfer	–	0.001_{1}	–	-0.024_{4}	–	
$E_{a,2}$	Total	6.37_{29}	6.42_{33}	3.45_{70}	4.53_{44}	4.12_{10}	3.7,[47] 4.1[54]
	Kinetic Energy	1.13_{11}	1.23_{21}	1.01_{34}	1.49_{11}	1.21_{5}	
	Lennard-Jones	-5.55_{59}	-5.75_{86}	-1.23_{47}	-1.38_{45}	-1.28_{8}	
	Coulombic	$19.6_{1.6}$	$19.4_{2.2}$	$4.7_{1.1}$	6.0_{7}	4.19_{14}	
	Polarization	-8.77_{71}	$-8.45_{1.02}$	-1.03_{28}	-1.53_{22}	–	
	Charge Transfer	–	0.001_{3}	–	-0.022_{8}	–	
$E_{a,D}$	Total	5.84_{36}	5.73_{15}	3.35_{9}	4.14_{13}	4.10_{5}	4.2-4.6[55–59]
	Kinetic Energy	1.23_{9}	1.21_{16}	1.04_{5}	1.17_{6}	1.16_{4}	
	Lennard-Jones	-5.04_{64}	-4.59_{25}	-1.16_{16}	-1.76_{15}	-1.24_{5}	
	Coulombic	$17.5_{1.7}$	16.1_{6}	4.53_{29}	6.27_{25}	4.18_{6}	
	Polarization	-7.81_{76}	-7.00_{29}	-1.06_{10}	-1.52_{5}	–	
	Charge Transfer	–	-0.002_{5}	–	-0.023_{10}	–	

TABLE II: Activation energies (in kcal/mol) for the H-bond exchange time ($E_{a,0}$), the OH reorientation time ($E_{a,2}$), and the water diffusion coefficient ($E_{a,D}$). Contributions from the kinetic energy and different interactions are shown in addition to the total value, which is compared to experimental values (with uncertainties of ±0.5 kcal/mol) where available. Subscripts indicate uncertainties in the trailing digit(s).

tween both molecules in the bifurcated H-bond. The loss of charge transfer energy between the H-bond donor and original acceptor is largely compensated by the gain in charge transfer energy with the new acceptor.

This does not mean that charge transfer is not coupled to dynamics, just not the H-bond exchange barriers. Using a similar CT treatment that eliminates CT beyond a distance of 2.8 Å, Sidler, *et al.*[28] showed that the charge of a molecule changes as it undergoes translational motion. Other studies using *ab initio* methods have found similar results.[25–27] Our results indicate that charge transfer, as implemented in the models used here, does not influence the dynamical barrier. That is, while the hindered translational and rotational motion of an H-bonded water will change the charge of the molecule, the charges must not be largely different at the transition states.

The polarization energy represents a large contribution to the total energy, about 5.5 kcal/mol per molecule for the FQ models and 3.3 kcal/mol per molecule for the Drude models. Polarization represents a significant contribution to the activation energy, acting in opposition to the Coulombic interactions. The significant and negative contribution indicates that the ability of the charges to change during H-bond exchanges decreases the time scales for motion. Note that the polarization energy is that required to polarize the molecules in the system and thus the combination of the Coulombic and polarization contributions can be reasonably viewed as the net electrostatic component. For the Drude-DCT model, we see $E_{a,0}^{Coul}+E_{a,0}^{Pol} = 3.90$ kcal/mol, while the SWM4-NDP description gives a smaller value of 3.16 kcal/mol. The negative Lennard-Jones contributions partially cancel these. The net electrostatic and Lennard-Jones values are in reasonable quantitative accord with previous results for fixed-charge models.[60] In contrast, the TIP4P-FQ-based models have a much larger net electrostatic contribution to $E_{a,0}$ around 9.4 kcal/mol. The Lennard-Jones contributions, $E_{a,0}^{LJ}$ are also greater in magnitude, moderating this dramatically increased electrostatic effect to yield a more modestly larger $E_{a,0}$.

In previous studies of fixed-charge water models we have found a key motif of competition between Coulombic and Lennard-Jones interactions.[9,10] The former provide a positive contribution to $E_{a,0}$, which is partially cancelled by the negative contribution of the latter. This behavior is representative of the H-bond description within these models: The H-bond is held together by the favorable electrostatic interactions that are balanced by the Lennard-Jones repulsion that prevents collapse of the two molecules. To break an H-bond the system must give up the favorable Coulombic interaction (raise that energy) while sliding down the repulsive wall of the Lennard-Jones potential (lowering that energy). It is not *a priori* obvious that this behavior would persist in polarizable models, but in fact it does, as discussed in the previous paragraph and illustrated by the results in Table II and Fig. 4.

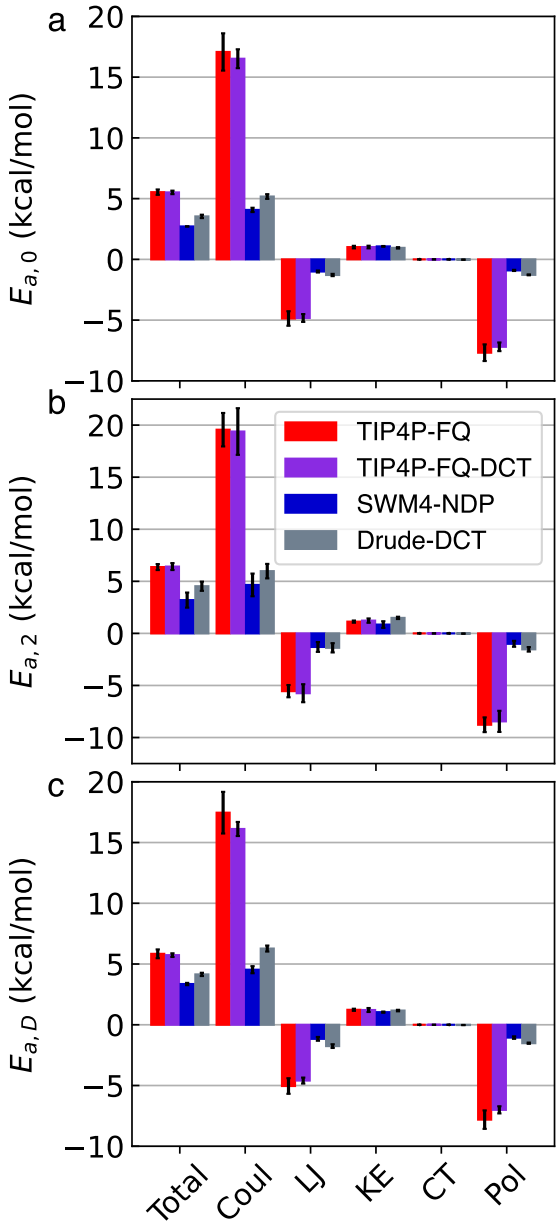

FIG. 4: Comparison of the activation energies and components from the kinetic energy and different interactions for the H-bond jump time, $E_{a,0}$, OH reorientation time, $E_{a,2}$, and water diffusion coefficient, $E_{a,D}$.

C. OH Reorientation Dynamics

A key manifestation of the H-bond exchange dynamics is in OH reorientation. Unlike the former, the timescales for OH reorientation dynamics can be obtained from experiments. Specifically, the OH reorientation dynamics expressed in the second-order TCF,

$$C_2(t) = \langle P_2[\vec{e}_{OH}(0)\cdot\vec{e}_{OH}(t)]\rangle, \tag{12}$$

where P_2 is the second-Legendre polynomial, can be determined from pump-probe infrared anisotropy[62] measurements, which can directly yield $0.4\,C_2(t)$. For water, $C_2(t)$ decays on three timescales, the longest of which, τ_2, is related to H-bond making and breaking and will be the focus here. Importantly, Laage and Hynes have shown that OH reorientation can be mechanistically and quantitatively described by an extended jump model (EJM).[40,41] Specifically, OH reorientation occurs *via* large-amplitude, $\sim 70°$, angular jumps associated with H-bond exchanges combined with reorientation of the intact H-bonded pair in between these jumps. Thus, the EJM gives $\tau_2^{-1} = \tau_{2,jump}^{-1} + \tau_{2,frame}^{-1}$, where $\tau_{2,jump}$ is a product of the H-bond jump time τ_0 and a geometric factor accounting for the size of the angular jump and $\tau_{2,frame}$ is the timescale for intact H-bond reorientation.

Thus, reorientation dynamics are perhaps the closest connection between an experimentally accessible property and H-bond exchanges. We have previously evaluated the activation energies for τ_2 itself, $E_{a,2}$, compared to the contributions of all of the EJM components,[10] confirming the accuracy of the EJM for describing not only reorientation timescales but also activation energies. Moreover, we found that the the jump time activation energy, $E_{a,0}$, is not equivalent to $E_{a,2}$ which has significant contributions from the frame reorientation activation energy. However, $E_{a,0}$ and $E_{a,2}$ tend to be fairly similar (with the latter typically larger) because the frame reorientation is also ultimately determined by H-bond exchanges in the surroundings and thus has an activation energy similar to that of the jump time itself.

With that prologue as context, we now consider the reorientation dynamics of the four polarizable and charge transfer water models. The calculated $C_2(t)$ TCFs are shown as a function of time in Fig. 5a and the reorientation times are given in Table I. The reorientation times are obtained by fitting $C_2(t)$ to a normalized, tri-exponential with τ_2 the longest timescale. With the exception of the SWM4-NDP model, which gives faster dynamics, the force fields yield reorientation times that are longer than the experimental value of 2.6 ps for isotopically dilute water.[47–49] These results are consistent with the trends observed for the H-bond jump times.

The temperature derivative of the reorientational TCF is calculated from the fluctuation theory approach described in Sec. II. That is,

$$\begin{aligned}\frac{\partial C_2(t)}{\partial\beta} &= -\langle \delta H(0)\, P_2[\vec{e}_{OH}(0)\cdot\vec{e}_{OH}(t)]\rangle \\ &\equiv -C_{2,H}(t).\end{aligned} \tag{13}$$

These derivative TCFs are shown for the four water models in Fig. 5b. In practice, $E_{a,2}$ is determined by fitting $C_{2,H}(t)$ to the derivative of the tri-exponential form assumed for $C_2(t)$; details of this approach can be found in Refs. 7 or 10. The activation energies are given in Table II along with the contributions from the kinetic energy and different interactions, which are all plotted in Fig. 4. Note that the activation energy and OH orienta-

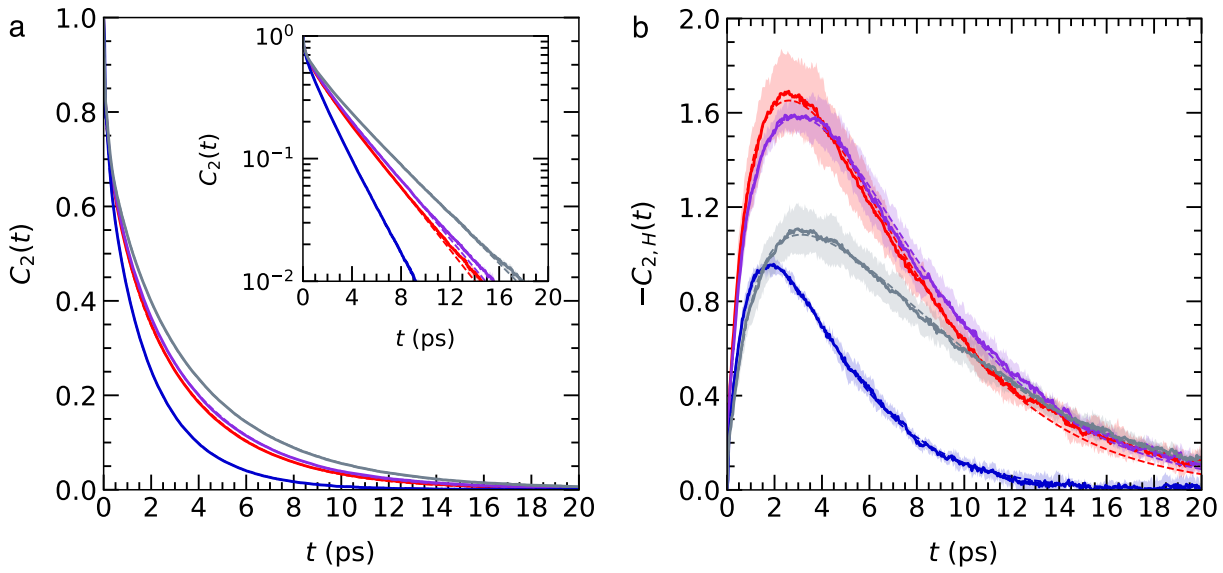

FIG. 5: The OH reorientational TCF, $C_2(t)$, is plotted as a function of time for the TIP4P-FQ (red), TIP4P-FQ-DCT (violet), SWM4-NDP (blue), and Drude-DCT (grey) models. Dashed lines of the same color show tri-exponential fits. Inset shows the TCFs on a semi-log scale. Shaded areas represent the 95% confidence intervals.

tion time is less for the SWM4-NDP model than the others, likely because only that model has gas-phase charges on the hydrogens (*vide supra*).

Qualitatively, the reorientational activation energies and their components mirror those for the H-bond jump time. However, $E_{a,2}$ is larger by ~ 1 kcal/mol for the Drude-DCT and TIP4P-FQ-based models, but only by 0.22 kcal/mol for the SWM4-NDP model. In the context of the EJM, this suggests the former may have differences in their descriptions of frame reorientation. Both the SWM4-NDP and Drude-DCT models give activation energies that are consistent with the measured values of 3.7 ± 0.5 and 4.1 ± 0.5 kcal/mol.[47,54] The TIP4P-FQ-based models have $E_{a,2}$ values that are significantly too large.

The contributions to $E_{a,2}$ exhibit the same negligible charge transfer effects, modest kinetic energy component, and significant electrostatic-Lennard-Jones competition as observed for the jump time activation energy. The key difference with the jump time results is that the magnitudes of the Coulombic, polarization, and Lennard-Jones contributions are all larger. In the context of the EJM, these changes must be attributable to the temperature dependence of the jump angle (which is likely to be a small effect[10]), the frame reorientation time, or even the relative contribution of the frame and jump components determined by the relative magnitude of the frame and jump times themselves. Determining the role of each these possibilities requires a detailed investigation beyond the scope of the present work.

D. Diffusion

Finally, we consider the water diffusion coefficient, which can also be probed experimentally.[50,55–59] It has recently been shown that water self-diffusion, like OH reorientation, can be understood as a combination of translational jumps associated with H-bond exchanges and diffusion of the water molecule in its intact H-bonded state between jumps.[42] Thus, the diffusion coefficient activation energy, $E_{a,D}$, has contributions from the activation energies of the H-bond jump time and frame (intact, H-bonded) diffusion coefficient as well as the temperature dependence of the translational jump amplitude.

We have calculated the water self-diffusion coefficient, D, from the mean-squared displacement,

$$MSD(t) = \langle |\vec{r}(t) - \vec{r}(0)|^2 \rangle. \tag{14}$$

At longer times the MSD is linear and, in practice, we obtain D as one-sixth the slope determined from a linear fit over the $10 - 20$ ps time interval. The MSDs for the four water models and associated fits are shown in Fig. 6a and the resulting diffusion coefficients are given in Table I. Corrections to D for finite-size effects have not been included;[51,52] applying this correction in reverse to the experimental value suggests an "uncorrected" experimental D of $\sim 2 \times 10^{-5}$ cm^2/s.[53] Consistent with the τ_2 results, the TIP4P-FQ, TIP4P-FQ-DCT, and Drude-DCT models give diffusion coefficients that are too slow relative to experiment, while the SWM4-NDP force field gives a D that is too large. However, the deviations from measured values are a bit more modest for diffusion than for the reorientation time.

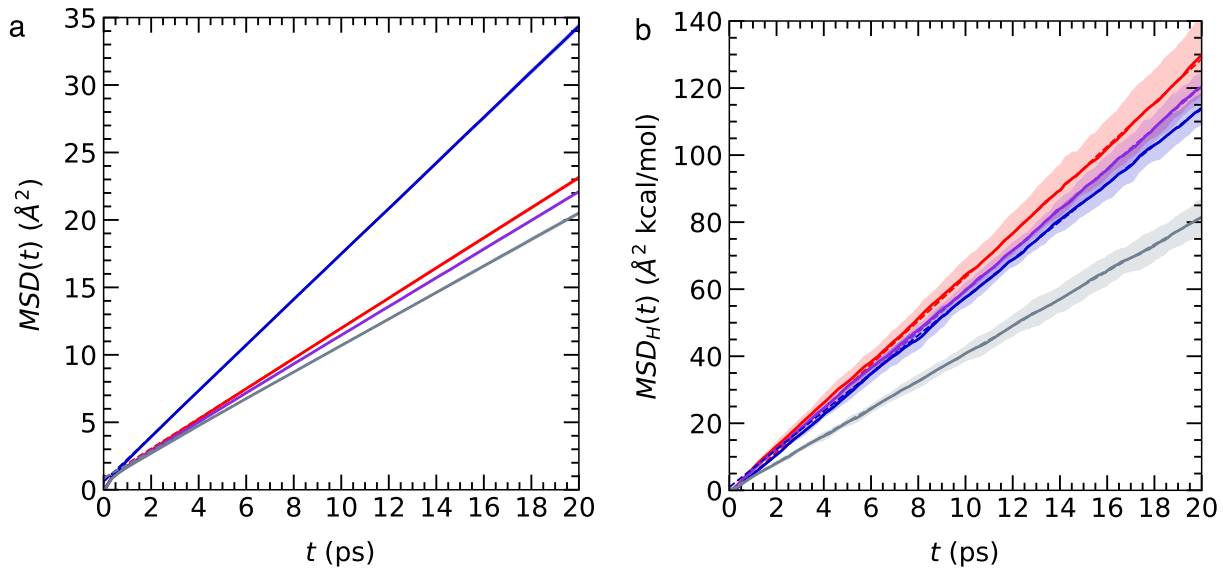

FIG. 6: The a) mean-squared-displacement, $MSD(t)$, and b) weighted mean-squared displacement, $MSD_H(t)$, are shown as a function of time for the TIP4P-FQ (red), TIP4P-FQ-DCT (violet), SWM4-NDP (blue), and Drude-DCT (grey) models. Dashed lines of the same color show linear fits over the data from $10-20$ ps. Shaded areas represent the 95% confidence intervals.

The diffusion coefficient activation energy, $E_{a,D}$, is obtained from the fluctuation theory approach in Sec. II in which the temperature derivative of the MSD is given by

$$\frac{\partial MSD(t)}{\partial \beta} = -\langle \delta H(0)\, |\vec{r}(t)-\vec{r}(0)|^2 \rangle, \equiv -MSD_H(t). \quad (15)$$

Analogous expressions apply to the contributions to the derivative from the kinetic energy and different interactions. The activation energy is then given by the ratio of the slope of $MSD_H(t)$ at long times (over the $10-20$ ps interval) to that of the $MSD(t)$ slope. The calculated $MSD_H(t)$ are shown in Fig. 6b along with the linear fits and the activation energies, and their components, are provided in Table II and shown in Fig. 4.

The activation energies are generally consistent with those for the H-bond jump and OH reorientation times. They are larger than the latter, but smaller than the former. This reflects the additional contributions above the jump time activation energy associated with the frame diffusion of the H-bonded water and the temperature dependence of the translational jumps. But it also suggests that these additions are smaller than the analogous ones for OH reorientation. Compared to the measured activation energy, the TIP4P-FQ and TIP4P-FQ-DCT models give $E_{a,D}$ values that are ~ 1 kcal/mol too large while the SWM4-NDP model yields a result too small by roughly the same amount. The Drude-DCT force field has a diffusion activation energy that agrees with the experimental value (within error bars).

The components of $E_{a,D}$ exhibit the same features as those for $E_{a,0}$, and $E_{a,2}$. Namely, the kinetic energy contribution is modest, ~ 1.1 kcal/mol, the charge transfer component is negligible, and the Coulombic contribution is the dominant one. The same competition between the positive net electrostatic ($E^{Coul}_{a,D} + E^{Pol}_{a,D}$) and the negative Lennard-Jones components, observed for the jump and reorientation times, is also operative for diffusion. This is indicative of the central role of H-bond making and breaking in these three dynamical timescales and the essential tension between attractive electrostatic and short-ranged repulsive forces in H-bonding.

V. CONCLUSIONS

We have calculated the dynamical timescales and activation energies for H-bond exchange, OH reorientation, and self-diffusion in liquid water within two polarizable and two polarizable plus charge-transfer models. The TIP4P-FQ, TIP4P-FQ-DCT, and Drude-DCT models yield dynamics that are too slow compared to measured values, while the SWM4-NDP force field predicts dynamics that are too fast.

It is interesting to examine these results in the context of the associated activation energies. For example, the Drude-DCT OH reorientation time and water diffusion coefficient are slower than those for the TIP4P-FQ-based models, which are, in turn, slower than the measured results. However, the activation energies for the Drude-DCT model for those same timescales are in agreement with experimental values, while the TIP4P-FQ-based force fields give activation energies that are

too large by $1-2$ kcal/mol (Table II). This suggests a significant role for energy-entropy compensation.

Indeed, evidence of this effect is also observed in the thermodynamics underlying the O-O radial distribution function; see Fig. 2. The four water models give RDFs that are quite similar, such that the corresponding O-O potentials of mean force differ by less than 0.2 kcal/mol. Yet, the internal energy profiles are dramatically different between the TIP4P-FQ-based models and the SWM4-NDP and Drude-DCT ones; the barrier to leave the first solvation shell for the former two is more than twice that for the latter two. However, the larger internal energy barriers are almost completely cancelled by the entropy, which is also of significantly greater magnitude for the TIP4P-FQ-based models. Note that this cancellation of very different internal energy and entropy profiles to yield very similar free energies and RDFs *at room temperature* will lead to divergent behavior of the models with temperature.

These results indicate flexibility in parameterizing a water model, by exploiting the energy-entropy compensation to yield accurate structure and dynamics at room temperature. At the same time, they point to the importance of including temperature dependent data to correctly reproduce the energetic barriers determining water dynamics. These lessons apply to both fixed-charge and polarizable models.

In previous studies, we have observed that water activation energies in fixed-charge and three-body water models result from a competition between contributions from the electrostatic and Lennard-Jones contributions.[7–10] The former are the driving force for the formation of H-bonds while the repulsive part of the latter prevent the water molecules from approaching too closely. Thus, to break an H-bond the electrostatic energy must increase while the Lennard-Jones energy decreases (moving down the repulsive wall). This leads to a positive electrostatic contribution to activation energies for water dynamics that is partially cancelled by a negative Lennard-Jones component. A key question addressed by this work is whether this behavior persists in water models that include polarization and charge transfer. The present results show that the answer is clearly yes. The same electrostatic-van der Waals competition is observed in all the models considered here. Thus, this appears to be a general feature of water models, be they fixed-charge, many-body, polarizable, or charge transfer.

ACKNOWLEDGMENTS

This work was supported by the National Science Foundation under Grant CHE-2102656 (W.H.T). The calculations were performed at the University of Kansas Center for Research Computing (CRC), including including the BigJay cluster resource funded through NSF Grant MRI-2117449.

DATA AVAILABILITY

The data that support the findings of this study are available from the corresponding author upon reasonable request.

[1] H. J. Berendsen, J. R. Grigera, and T. P. Straatsma, "The missing term in effective pair potentials," J. Phys. Chem **91**, 6269–6271 (1987).
[2] W. L. Jorgensen, J. Chandrasekhar, J. D. Madura, R. W. Impey, and M. L. Klein, "Comparison of simple potential functions for simulating liquid water," J. Chem. Phys. **79**, 926–935 (1983).
[3] M. W. Mahoney and W. L. Jorgensen, "A five-site model for liquid water and the reproduction of the density anomaly by rigid, nonpolarizable potential functions," J. Chem. Phys. **112**, 8910–8922 (2000).
[4] H. W. Horn, W. C. Swope, J. W. Pitera, J. D. Madura, T. J. Dick, G. L. Hura, and T. Head-Gordon, "Development of an improved four-site water model for biomolecular simulations: TIP4P-Ew," J. Chem. Phys. **120**, 9665–9678 (2004).
[5] S. W. Rick, "A reoptimization of the five-site water potential (TIP5P) for use with Ewald sums," J Phys Chem **120**, 6085–6093 (2004).
[6] S. Izadi and A. V. Onufriev, "Accuracy limit of rigid 3-point water models," J. Chem. Phys. **145**, 074501 (2016).
[7] Z. A. Piskulich, O. O. Mesele, and W. H. Thompson, "Removing the barrier to the calculation of activation energies: Diffusion coefficients and reorientation times in liquid water," J. Chem. Phys. **147**, 134103 (2017).
[8] Z. A. Piskulich, O. O. Mesele, and W. H. Thompson, "Activation energies and beyond," J. Phys. Chem. A. **123**, 7185–7194 (2019).
[9] Z. A. Piskulich and W. H. Thompson, "Examining the role of different molecular interactions on activation energies and activation volumes in liquid water," J. Chem. Theory Comput. **17**, 2659–2671 (2021).
[10] Z. A. Piskulich, D. Laage, and W. H. Thompson, "Activation energies and the extended jump model : How temperature affects reorientation and hydrogen-bond exchange dynamics in water," J. Chem. Phys. **153**, 074110 (2020).
[11] P. Cieplak, P. A. Kollman, and T. P. Lybrand, "A new water potential including polarization: application to gas-phase, liquid, and crystal properties of water," J. Chem. Phys. **92**, 6755–6760 (1990).
[12] S. W. Rick, S. J. Stuart, and B. J. Berne, "Dynamical fluctuating charge force fields: Application to liquid water," J. Chem. Phys. **101**, 6141–6156 (1994).
[13] L. X. Dang and T. Chang, "Molecular dynamics study of water clusters, liquid, and liquid-vapor interface of water with many-body potentials," J. Chem. Phys. **106**, 8149–8159 (1997).
[14] P. Ren and J. W. Ponder, "Polarizable atomic multipole water model for molecular mechanics simulation," J. Phys. Chem. B **107**, 5933–5947 (2003).
[15] G. Lamoureux, E. Harder, I. V. Vorobyov, B. Roux, and A. D. MacKerell, Jr., "A polarizable model of water for molecular dynamics simulations of biomolecules," Chem. Phys. Lett. **418**, 245–249 (2006).
[16] A. Holt, J. Boström, G. Karlström, and R. Lindh, "A nemo potential that includes the dipole-quadrupole and quadrupole-quadrupole polarizability," J. Comput. Chem. **31**, 1583–1591 (2010).
[17] P. Cieplak, F.-Y. Dupradeau, Y. Duan, and J. Wang, "Polarization effects in molecular mechanical force fields," J. Phys. – Condens. Mat. **21**, 333102 (2009).
[18] C. Millot, J.-C. Millot, J.-C. Soetens, M. T. C. Martins Costa, M. P. Hodges, and A. J. Stone, "Revised anisotropic site potentials for the water dimer and calculated properties," J. Phys. Chem A **102**, 754–770 (1998).

[19]K. Honda, "An effective potential function with enhanced charge-transfer-type interaction for hydrogen-bonding liquids," J. Chem. Phys. **117**, 3558–3569 (2002).
[20]R. Chelli, M. Pagliai, P. Procacci, G. Cardini, and V. Schettino, "Polarization response of water and methanol investigated by a polarizable force field and density functional theory calculations: Implications for charge transfer," J. Chem. Phys. **122**, 074504 (2005).
[21]J. Piquemal, J. Chevreau, and N. Gresh, "Toward a separate reproduction of the contributions to the Hartree-Fock and DFT intermolecular interaction energies by polarizable molecular mechanics with the SIBFA potential," J. Chem. Theory Comput. **3**, 824–937 (2007).
[22]R. Kumar, F. F. Wang, G. R. Jenness, and K. D. Jordan, "A second generation distributed point polarizable water model," J. Chem. Phys. **132**, 014309 (2010).
[23]A. J. Lee and S. W. Rick, "The effects of charge transfer on the properties of liquid water," J. Chem. Phys. **134**, 184507 (2011).
[24]S. W. Rick, "A polarizable, charge transfer model of water using the drude oscillator," J. Comput. Chem. **37**, 2060–2066 (2016).
[25]M. Sharma, R. Resta, and R. Car, "Intermolecular dynamical charge fluctuations in water: A signature of the H-bond network," Phys. Rev. Lett. **95**, 187401 (2005).
[26]H. Torii, "Intermolecular electron density modulations in water and their effects on the far-infrared spectral profiles at 6 THz," J. Phys. Chem. B **115**, 6636–6643 (2011).
[27]Q. Wan, L. Spanu, G. Galli, and F. Gygi, "Vibrational signatures of charge fluctuations in the hydrogen bond network of liquid water," J. Chem. Theory Comput. **9**, 4124–4130 (2013).
[28]D. Sidler, M. Meuwly, and P. Hamm, "An efficient water force field calibrated against intermolecular THz and Raman spectra," J. Chem. Phys. **148**, 244504 (2018).
[29]H. Xu, H. A. Stern, and B. Berne, "Can water polarizability be ignored in hydrogen bond kinetics?" J. Chem. Phys. B **106**, 2054–2060 (2002).
[30]H. Kumar, C. Dasgupta, and P. K. Maiti, "Structure, dynamics and thermodynamics of single-file water under confinement: Effects of polarizability of water molecules," RSC Adv. **5**, 1893–1901 (2015).
[31]M. Sprik, "Computer simulation of the dynamics of induced polarization fluctuations in water," J. Phys. Chem. **95**, 2283–2291 (1991).
[32]K. Watanabe and M. L. Klein, "Effective pair potentials and the properties of water," Chem. Phys. **131**, 157–167 (1989).
[33]O. O. Mesele and W. H. Thompson, "Removing the barrier to the calculation of activation energies," J. Chem. Phys. **145**, 13410 (2016).
[34]J. Korchowiec and T. Uchimaru, "New energy partitioning scheme based on the self-consistent charge and configuration method for subsystems: Application to water dimer system," J. Chem. Phys. **112**, 1623 (2000).
[35]O. Gálvez, P. C. Gómez, and L. F. Pacios, "Variation with the intermolecular distance of properties dependent on the electron density in hydrogen bond dimers," J. Chem. Phys. **115**, 11166–1184 (2001).
[36]M. P. Allen and D. J. Tildesley, *Computer Simulation of Liquids* (Oxford Univerity, 1987).
[37]G. Lamoureux and B. Roux, "Modelling induced polarization with classical drude oscillators: theory and molecular dynamics simulation algorithm," J. Chem. Phys. **119**, 3025–3039 (2003).
[38]D. P. Shoemaker, C. W. Garland, and J. W. Nibler, *Experiments in Physical Chemistry* (McGraw-Hill, New York, 1989).
[39]Z. A. Piskulich and W. H. Thompson, "On the temperature dependence of liquid structure," J. Chem. Phys. **152**, 011102 (2020).
[40]D. Laage and J. T. Hynes, "A molecular jump mechanism of water reorientation," Science **311**, 832–835 (2006).
[41]D. Laage and J. T. Hynes, "On the molecular mechanism of water reorientation." J. Phys. Chem. B **112**, 14230–14242 (2008).
[42]A. Gomez, Z. A. Piskulich, W. H. Thompson, and D. Laage, "Water diffusion proceeds via a hydrogen-bond jump exchange mechanism," J. Phys. Chem. Lett. **13**, 4660–4666 (2022).
[43]Z. A. Piskulich, D. Laage, and W. H. Thompson, "On the role of hydrogen-bond exchanges in the spectral diffusion of water," J. Chem. Phys. **154**, 064501 (2021).
[44]R. F. Grote and J. T. Hynes, "The stable states picture of chemical reactions. II. Rate constants for condensed and gas phase reaction models," J. Chem. Phys. **73**, 2715–2732 (1980).
[45]C. J. Tainter, P. A. Pieniazek, Y. S. Lin, and J. L. Skinner, "Robust three-body water simulation model," J. Chem. Phys. **134**, 184501 (2011).
[46]C. J. Tainter, L. Shi, and J. L. Skinner, "Reparametrized E3B (explicit three-body) water model using the TIP4P/2005 model as a reference," J. Chem. Theory Comput. **11**, 2268–2277 (2015).
[47]C. Petersen, K. J. Tielrooij, and H. J. Bakker, "Strong temperature dependence of water reorientation in hydrophobic hydration shells," J. Chem. Phys. **130**, 214511 (2009).
[48]D. E. Moilanen, E. E. Fenn, Y.-S. Lin, J. L. Skinner, B. Bagchi, and M. D. Fayer, "Water inertial reorientation: Hydrogen bond strength and the angular potential," Proc. Natl. Acad. Sci. USA **105**, 5295–5300 (2008).
[49]K. Ramasesha, S. T. Roberts, R. A. Nicodemus, A. Mandal, and A. Tokmakoff, "Ultrafast 2D IR anisotropy of water reveals reorientation during hydrogen-bond switching," J. Chem. Phys. **135**, 054509 (2011).
[50]H. Weingartner, "Self-Diffusion in liquid water. A reassessment," Z. Phys. Chem. **132**, 129–149 (1982).
[51]B. Dunweg and K. Kremer, "Molecular dynamics simulation of a polymer chain in solution," J. Chem. Phys. **99**, 6983–6997 (1993).
[52]I. C. Yeh and G. Hummer, "System-size dependence of diffusion coefficients and viscosities from molecular dynamics simulations with periodic boundary conditions," J. Phys. Chem. B. **108**, 15873–15879 (2004).
[53]For comparison to experiment, with the box size used in these simulations (~ 21.6 Å), and using the experimental shear viscosity (8.903×10^{-4} kg/m^{-1}s^{-1}), the correction for the finite size of the simulation cell would is $\sim 0.3 \times 10^{-5}$ cm^2/s. Thus, a value of $\sim 2 \times 10^{-5}$ cm^2/s would be in agreement with experiment.
[54]R. A. Nicodemus, S. A. Corcelli, J. L. Skinner, and A. Tokmakoff, "Collective hydrogen bond reorganization in water studied with temperature-dependent ultrafast infrared spectroscopy," J. Phys. Chem. B. **115**, 5604–5616 (2011).
[55]L. A. Woolf, "Tracer diffusion of tritiated water (THO) in ordinary water (H_2O) under pressure," J. Chem. Soc., Faraday Trans. 1 **71**, 784–796 (1975).
[56]R. Mills, "Self-diffusion in normal and heavy water in the range $1 - 45°$," J. Phys. Chem. **77**, 685–688 (1973).
[57]K. Krynicki, C. D. Green, and D. W. Sawyer, "Pressure and temperature dependence of self-diffusion in water," Faraday Discuss. Chem. Soc. **66**, 199–208 (1978).
[58]K. T. Gillen, D. C. Douglass, and M. J. Hoch, "Self-diffusion in liquid water to $-31°$C," J. Chem. Phys. **57**, 5117–5119 (1972).
[59]H. R. Pruppacher, "Self-diffusion coefficient of supercooled water," J. Chem. Phys. **56**, 101–107 (1972).
[60]Z. A. Piskulich and W. H. Thompson, "The dynamics of supercooled water can be predicted from room temperature simulations," J. Chem. Phys. **152**, 074505 (2020).
[61]E. Duboué-Dijon, A. C. Fogarty, and D. Laage, "Temperature dependence of hydrophobic hydration dynamics: From retardation to acceleration," J. Phys. Chem. B **118**, 1574–1583 (2014).
[62]Y. S. Lin, P. A. Pieniazek, M. Yang, and J. L. Skinner, "On the calculation of rotational anisotropy decay, as measured by ultrafast polarization-resolved vibrational pump-probe experiments," J. Chem. Phys. **132**, 174505 (2010).